ACS OMEGA

Open Access

http://pubs.acs.org/journal/acsodf

Article

Toward Nano- and Microplastic Sensors: Identification of Nano- and Microplastic Particles via Artificial Intelligence Combined with a Plasmonic Probe Functionalized with an Estrogen Receptor

Mimimorena Seggio,*[,§] Francesco Arcadio,[§] Eros Radicchi, Nunzio Cennamo, Luigi Zeni, and Alessandra Maria Bossi

Cite This: *ACS Omega* 2024, 9, 18984−18994

Read Online

ACCESS | Metrics & More | Article Recommendations | Supporting Information

ABSTRACT: Nano- and microplastic particles are a global and emerging environmental issue that might pose potential threats to human health. The present work exploits artificial intelligence (AI) to identify nano- and microplastics in water by monitoring the interaction of the sample with a sensitive surface. An estrogen receptor (ER) grafted onto a gold surface, realized on a nonexpensive and easy-to-produce plastic optical fiber (POF) platform in order to excite a surface plasmon resonance (SPR) phenomenon, has been developed in order to carry out a "smart" sensitive interface (ER−SPR−POF interface). The ER−SPR−POF interface offers output data useful for exploiting a machine learning-based approach to achieve nano- and microplastic particle sensors. This work developed a proof-of-concept sensor through a training phase carried out by different particles, in terms of materials and size. The experimental results have demonstrated that the proposed "smart" ER−SPR−POF interface combined with AI can be used to identify the kind of particles in terms of the materials (polystyrene; poly(methyl methacrylate)) and size (20 μm; 100 nm) with an accuracy of 90.3%.

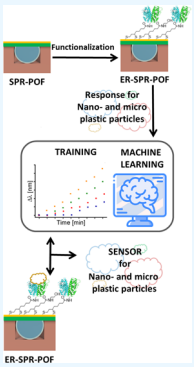

1. INTRODUCTION

Artificial intelligence (AI) sensing is an evolving technology that can provide groundbreaking solutions to several research areas, particularly when dealing with complex scenarios, such as in molecular diagnostics[1−3] and environmental pollution.[4] Indeed, AI-based techniques remarkably enhance sensor and biosensor technology, enabling to process and cluster huge amounts of data in real time, bringing out patterns, hence favoring fast and accurate decision-making. AI facilitates data merging, efficiently combining information from several sensors,[5] empowering an improved analytical identification of the samples. Lastly, by changing the hardware designs of traditional sensors to AI-based ones, holistic intelligent sensor systems can be devised.[6]

Traditional sensing pursues recognition elements (antibodies, enzymes, peptides, nucleic acids, molecular beacons, etc.), exhibiting the highest selectivity for a target analyte; thus, when coupled to a transducer (electrochemical, optical, piezoelectric, etc.), a specific and measurable signal is produced upon binding. For multiple molecular constituents in a solution or for the identification of a class of compounds with heterogeneous characteristics, such a traditional biosensor can be limited by a shortfall of specific recognition elements. As a possible solution, nowadays, researchers are developing biosensors that lack a specific recognition element;[6] instead, analyte-specific patterns in the signals are decoded by means of fingerprint techniques. Typical examples are the semispecific chemical sensor arrays, named E-nose, which have been developed for gas sensing, or E-tongue, which consists of an array of sensors for in-solution measurements.[7,8] Machine Learning (ML) techniques have been employed to recognize signal patterns that correlate to a particular analyte and hence to detect them, providing the required specificity.[9] Principal component analysis (PCA),[10] k-nearest-neighbors (KNN),[11] support vector machine (SVM),[12] artificial neural networks (ANN),[13,14] and other algorithms have shown outstanding performance in this frame.[9]

The highest impact of AI-based approaches stands in the detection of analytes with heterogeneous characteristics, for which it is difficult to find highly specific recognizing materials, such as in the epitomizing case of pollution caused by micrometric and submicrometric plastic particles. The micro- and nanoplastics appear to be a ubiquitous environmental problem and their presence has been reported in all biospheres, including freshwater, seawater, soil, and air,[15−20] posing a serious threat to health on the planet.[21] Indeed, despite the fact that plastics provide many benefits to modern society by bringing convenience to our daily lives,[22−24] only 9−40% are recycled[25] and as a result, most of the plastics are

Received: November 28, 2023
Revised: February 23, 2024
Accepted: February 28, 2024
Published: April 18, 2024

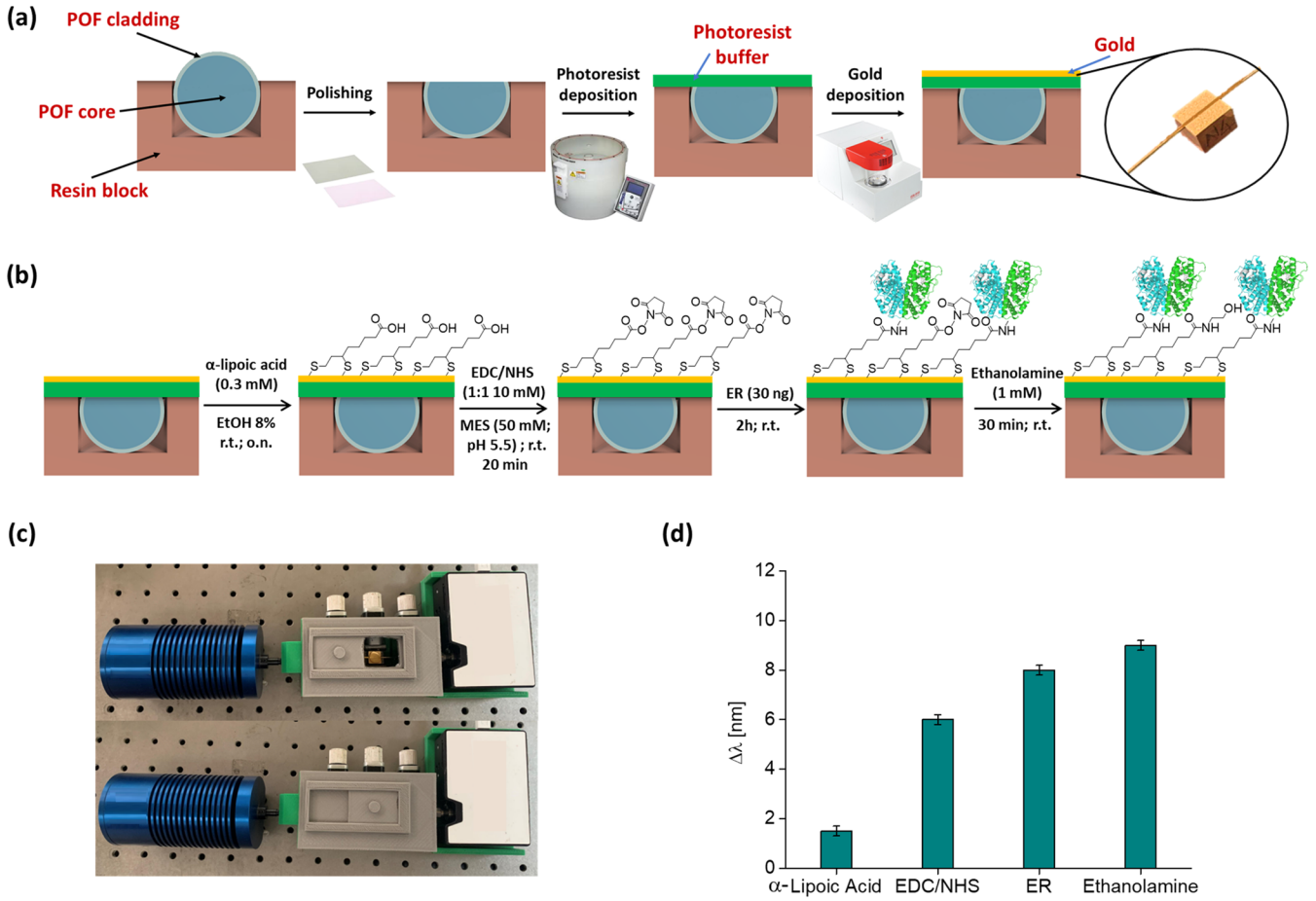

Figure 1. (a) Scheme of the SPR-POF platform production process. In the inset: the actual image of the obtained platform. (b) Scheme of coupling reactions with ER and (c) experimental setup of the ER−SPR−POF platform with an open (on the top) and capped lid (on the bottom). (d) Variation of the resonance wavelength, calculated with respect to the bare platform value, considering water as the surrounding medium, after each step of the functionalization process on ER−SPR−POF (n = 3, standard deviation (SD) = 0.15 nm).

indiscriminately discharged into the environment, becoming persistent wastes.

Plastic pollution is a complex scenario, with a classification organized in a primary source of pollutants, that comprises micro- and nanoplastics, manufactured for the most diverse uses in such a scale; and pollutants of a secondary source, which are micro- and nanoplastics debris originated from the cracking of macroplastics discharged in the environment, by the action of chemical and physical agents.[26,27]

In general, plastic particles are classified on the basis of their size into macro-, meso- (>5 mm), micro- (1 μm−5 mm), and nanoplastics (particles size <1 μm)[28] and on the basis of their constituent materials (polyethylene (PE); poly(methyl methacrylate) (PMMA); polystyrene (PS); poly(vinyl chloride) (PVC) etc.).[29] Indeed, given such a complexity, micro- and nanoplastic monitoring has proven to be a tough analytical challenge.[29,30]

Nowadays, conventional methods employed in micrometric plastics detection[31] provide partial information either about dimensions, i.e., scanning electron microscopy (SEM), transmission electron microscopy (TEM), and nanoparticle tracking analysis (NTA) or about the material, i.e., Fourier transform infrared spectroscopy and microscopy (FTIR) and mass spectrometry (MS).

However, a strategy for the rapid and "on-site" screening of micro- and nanoplastics in water samples without the need for expensive laboratory instruments and specialized staff is still in progress. Up to date, micro- and nanoplastics sensors have been developed by using electrochemical impedance spectroscopy (EIS) and amperometric and voltammetric techniques as comprehensively reported in a recent review.[32] In addition, standing the recent developments in the fabrication of three-dimensional (3D) freeform surfaces, deformable functional sensors/circuits and standalone stretchable sensing platforms could be useful in this frame.[33−37] The development of optical sensors could provide a solution to the environmental monitoring of micro- and nanoplastics.[38,39] Huang et al.[38] proposed for the first time the use of estrogen receptor (ER) as a recognizing element for plastic particles. However, in this case, the biosensor was solely tested for micrometric plastic particles in different materials (PS, PVC, PE), showing apparent dissociation constants ranging between 0.19 and 3.32 nM. Starting from these results, in our recent work,[40] the interaction of ER with nanometric plastic particles was studied using a nanoplasmonic platform, obtaining a biosensor that responds within the concentration range of the expected environmental loads without sample pretreatment. In the present work, as a proof of concept, an AI-based approach for the detection and classification of plastic particles in terms of size (micro-; nano-) and material (PMMA; PS) was proposed. To this purpose, the ER "smart" recognizing element[38] was grafted onto a nonexpensive and easy-to-produce D-shaped

https://doi.org/10.1021/acsomega.3c09485
ACS Omega 2024, 9, 18984−18994

plasmonic plastic optical fiber (POF) probe based on the Surface Plasmon Resonance (SPR) phenomenon.[41] The sensor was interrogated over time in order to record specific kinetic patterns for the different classes of plastic particles. The optical mapping over time of interaction of ER with plastic particles was used to provide a multiparametric description of the particle's characteristics in terms of the size and type of material. A subsequent AI training enabled to develop a prediction model for the sensor data set and to analyze the plastic content in water samples.

2. RESULTS

2.1. Functionalization Process of SPR−POF Probes. With the aim of producing a sensor capable of interacting with micro- and nanoplastics, an SPR−POF platform[41] was functionalized with the ER as a recognition element.[38] The preparation of the SPR-POF and its functionalization with ER are schematically reported in Figure 1a,1b, and described in detail in Sections 4.2 and 4.3, respectively, while the employed experimental setup is shown in Figure 1c. The sensor configuration was chosen for its low cost and simple setup, which is foreseen as ideal for in-field measurements. Concerning the cost analysis, it should be stressed that the ER−SPR−POF platforms cost about 5 USD each comprising material, machine, and process costs; the white light source is around 1000 USD, while the spectrometer costs around 3000 USD. Nevertheless, despite the fact that the instrumentation (white light source and spectrometer) represents a one-time cost, a cheaper light-emitting diode (LED) and a photodetector could be used in order to further reduce experimental setup costs.

In detail, the SPR−POF surface was functionalized with ER according to the protocol reported by Arcadio et al.[42] and optimized by Pasquardini et al.;[43] the coupling protocol consisted of a multistep procedure in which an α-lipoic acid self-assembled monolayer (SAM) was formed on the gold surface; subsequently, the carboxyl terminal moieties were activated with *N*-(3-(dimethylamino)propyl)-*N*′-ethylcarbodiimide hydrochloride/*N*-hydroxysuccinimide (EDC/NHS), and then the ER was covalently coupled to SAM. Finally, the surface was passivated with ethanolamine. Figure 1d reports the resonance wavelength shifts obtained with the setup depicted in Figure 1c (described in Section 4.5) after each step of the functionalization process outlined in Figure 1b. It was observed that the SPR wavelength variation ($\Delta\lambda$), calculated with respect to the value obtained by a bare surface and acquired with the same bulk (water, refractive index (RI) 1.332), showed a progressive increase (red shift) after each functionalization step (i.e., SAM, EDC/NHS, ER, passivation). In other words, the bulk solution (water) being fixed, the RI in contact with the plasmonic surface increases during the functionalization process. Furthermore, the success of the reactions was verified with an independent method through the attenuated total reflectance-FTIR (ATR-FTIR) characterization of the surface at different functionalization steps (bare surface, SAM, ER). As shown in Figure 2, although the bare surface does not show any relevant IR signal, the SAM and ER spectra confirm that the functionalization steps effectively took place.

Particularly, at least two distinctive features could be highlighted in the SAM spectrum, i.e., the C═O stretching at ∼1660 and ∼1540 cm^{-1} and the O−H stretching, from the weak broad band at ∼3300 cm^{-1}, both coming from the carboxylic group of the anchored α-lipoic acid molecules. Similarly, the same absorptions could be seen in the ER spectrum, plus additional signals reasonably pointing to the stretching of the C−O (∼1080 cm^{-1}) and N−H (∼3300 cm^{-1}) protein functional groups.

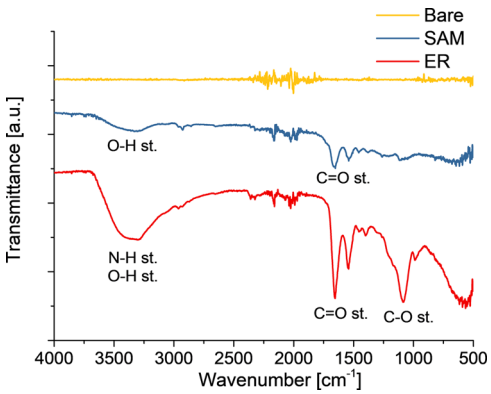

Figure 2. FTIR transmittance spectra of the bare surface (yellow), SAM (blue), and ER (red), with partial functional group assignation of the main absorption bands.

2.2. Binding Isotherm of the ER−SPR−POF Sensor for Micro- and Nanoplastics. In order to representatively differentiate the plastic particles in terms of both dimensions and materials, four types of plastic particles different in size and composition were selected: PMMA microplastics (20 μm), PS microplastics (20 μm), PMMA nanoplastics (100 nm), and PS nanoplastics (100 nm).

The response of the ER−SPR−POF biosensor to increasing particle concentrations (ranging from 1 to 10 mg/mL) was tested at 8 min of incubation time.

The resonance wavelength red-shifted for increasing concentrations of plastic particles (PMMA microplastics, PMMA nanoplastics, PS microplastics, and PS nanoplastics) as shown in the SPR spectra reported in Figure S1. As a control, bare platforms were tested in the same plastic particles' concentration range, and no $\Delta\lambda$s were observed (Figure S2). Figure 3 reports the binding isotherms for the different plastic particles tested (PMMA microplastics, PMMA nanoplastics, PS microplastics, and PS nanoplastics), in which the experimental data were fitted with the Hill model equation, which has the general formula herein reported (eq 1)

$$\Delta\lambda = \lambda_c - \lambda_0 = \Delta\lambda_{max}\cdot\left(\frac{c^n}{EC_{50}{}^n + c^n}\right) \quad (1)$$

where λ_c is the resonance wavelength at the analyte concentration c; λ_0 is the resonance wavelength in the absence of the analyte (blank); $\Delta\lambda_{max}$ is the maximum value of $\Delta\lambda$; calculated by subtracting the blank value from the saturation value; n is the Hill coefficient, and EC_{50} is the ligand concentration at half-saturation. The resulting parameters, obtained by Origin Pro 9 software, are listed in Table 1. This fitting model was chosen because it is apt to describe heterogeneous binding. Indeed, the sensor reported here is based on the ER recognition element, exploited to recognize non-natural ligands (nano- and microplastics), characterized by various sizes and compositions. On the contrary, when the receptor was tested for the binding to its own target (estradiol), the binding isotherm was described by a Langmuir model, as reported in Arcadio et al.[42]

https://doi.org/10.1021/acsomega.3c09485
ACS Omega 2024, 9, 18984−18994

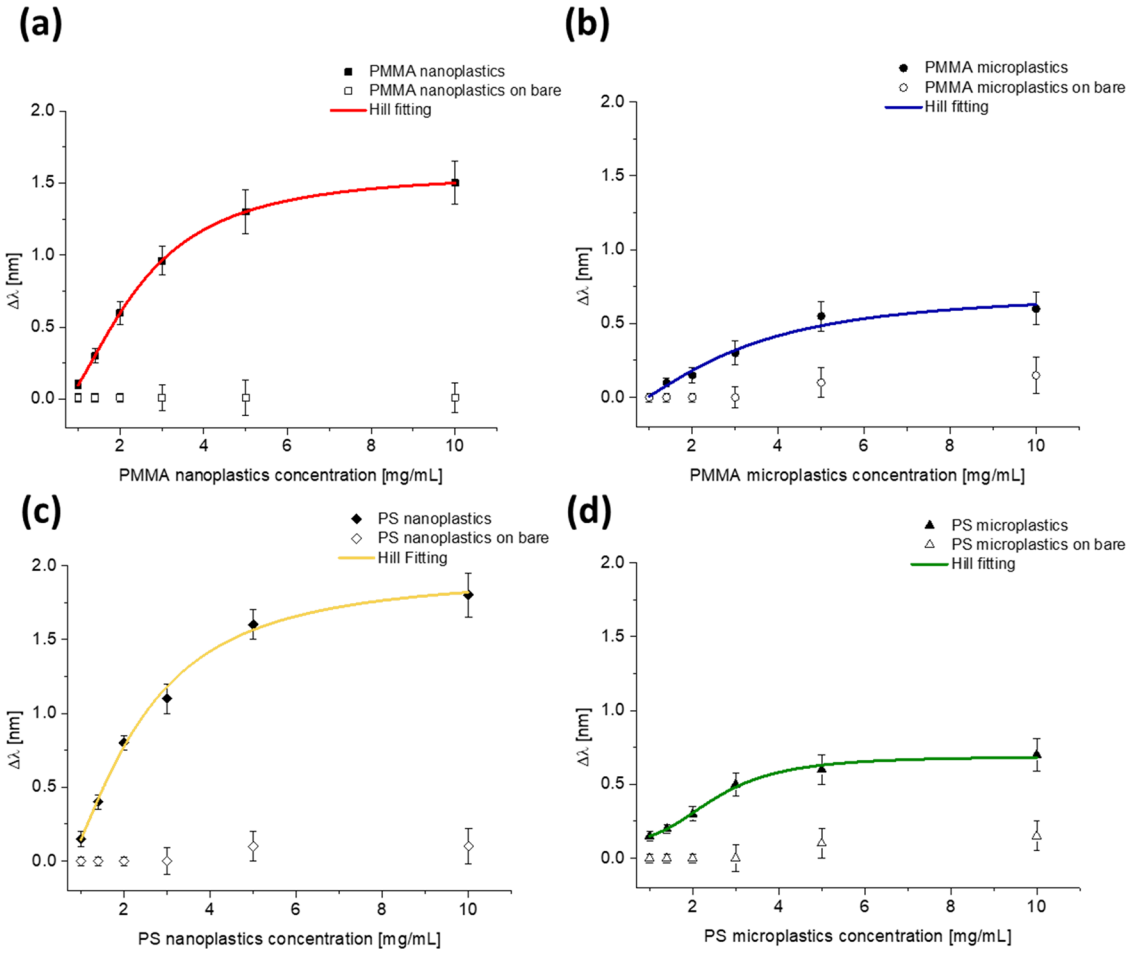

Figure 3. Variation in resonance wavelength as a function of (a) PMMA nanoplastics, (b) PMMA microplastics, (c) PS nanoplastics, and (d) PS microplastics concentrations on bare and functionalized platform and Hill fitting of the experimental data. The error bars were calculated as the SD of the data set (n = 3).

Table 1. ER−SPR−POF Fitting Parameters for Micro- and Nanoplastics

					statistics	
ER−SPR−POF	$\Delta\lambda_0$ [nm]	$\Delta\lambda_{max}$ [nm]	EC_{50} [mg/mL]	n	reduced χ^2	adj. R^2
PMMA nanoplastics	−0.17 ± 0.01	1.57 ± 0.01	2.23 ± 0.02	2.11 ± 0.02	0.01	0.999
PMMA microplastics	0.01 ± 0.05	0.62 ± 0.05	2.97 ± 0.32	3.15 ± 1.12	0.01	0.971
PS nanoplastics	−0.34 ± 0.20	1.94 ± 0.21	2.04 ± 0.27	1.82 ± 0.60	0.60	0.990
PS microplastics	0.12 ± 0.02	0.69 ± 0.03	2.52 ± 0.14	3.13 ± 0.55	0.19	0.991

Additionally, from the fitting parameters obtained by the Hill model equation, the sensitivity at low concentration (S_{lowc}) and the apparent binding affinity (K_{aff}) were calculated as reported in eqs 2 and 3, respectively

$$S_{lowc} = \Delta\lambda_{max}/EC_{50} \quad (2)$$

$$K_{aff} = 1/EC_{50} \quad (3)$$

Table 2 reports the S_{lowc} and K_{aff} values. From the EC_{50} value comparison, it is possible to deduce that the interaction between the ER-based recognition element and different types/sizes of plastic particles appears different, according to the results reported by Huang et al.[38] This discrepancy appears even more evident if the concentrations are converted from milligrams per milliliter to molar concentrations (see Section S3). The conversion was carried out in order to obtain an estimation of the number of moles and therefore of the number of particles contained in the samples. By comparing the fitting parameters obtained from the experimental value plotted as a function of plastic particles concentration calculated in mg/mL (reported in Table 1) and in molarity (reported in Table S1), it is possible to underline an amplified difference between the type of plastic particles, and a trend reversal of the EC_{50} linked to the correction as a function of the number of particles, which appear for microplastics

Table 2. ER−SPR−POF Sensitivity at Low Concentrations for Micro- and Nanoplastics Detection

ER−SPR−POF	S_{lowc} [nm/(mg mL^{-1})]	$K_{aff} = 1/EC_{50}$ [(mg/mL)$^{-1}$]
PMMA nanoplastics	0.70	0.45
PMMA microplastics	0.21	0.34
PS nanoplastics	0.95	0.95
PS microplastics	0.27	0.40

https://doi.org/10.1021/acsomega.3c09485
ACS Omega 2024, 9, 18984−18994

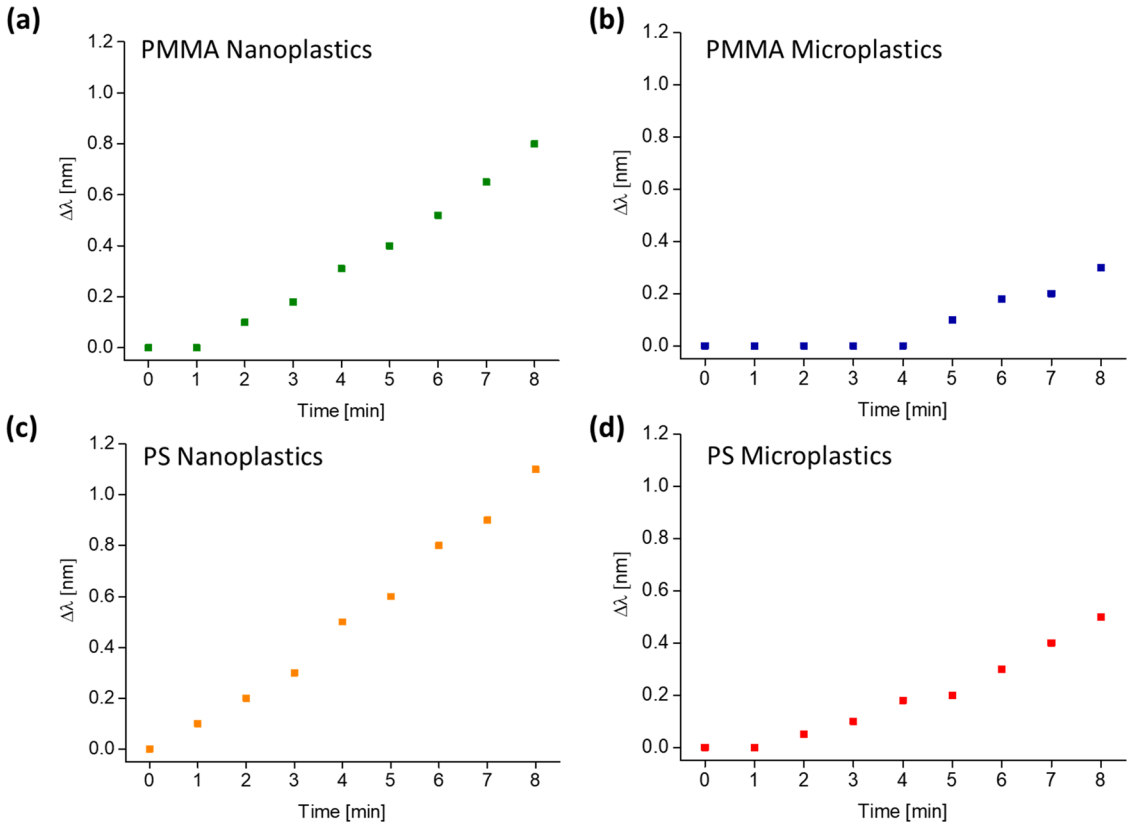

Figure 4. Variation in resonance wavelength ($\Delta\lambda$) as a function of incubation time for (a) PMMA nanoplastics, (b) PMMA microplastics, (c) PS nanoplastics, and (d) PS microplastics.

approximately 7 orders of magnitude smaller with respect to nanoplastics.

This reversal of trends also appears when calculating the K_{aff}. The K_{aff} of the tested plastic particles, by varying the material (PS and PMMA), showed a behavior in agreement with the results of interaction studies of synthetic polymers with biomacromolecules, such as the ER, as in Enyoh et al.,[44] showing a greater affinity for PS than PMMA. Instead, at different particle sizes, a higher K_{aff} value was obtained for microplastics compared to nanoplastics by expressing the K_{aff} in molar concentration, due to the larger size and the related multisite interaction (reported in Table S2). However, for an easier data treatment (i.e., avoiding to estimate the plastic particle's molecular weight), the apparent K_{aff} was expressed in mg/mL, in which there was a trend reversal (K_{aff} nanoplastic > K_{aff} microplastic) as reported in Table 1, due to the higher number of particles in nanoplastic samples compared to microplastics one for the same concentration calculated in mg/mL. Also, the different S_{lowc} confirmed the dissimilar interaction behavior of the tested plastic particles. In particular, the S_{lowc} appears different for nano- compared to microplastics and obtains better performances for PS compared to PMMA. Also in this case, the S_{lowc} is influenced by the method of reporting the concentration (i.e., molar concentration or mg/mL) for the same reason reported above for K_{aff}. The behavior for different particle sizes reports a larger S_{lowc} for microplastics compared to that for nanoplastics, calculating the S_{lowc} in molar concentration (as reported in Table S2). Instead, for the S_{lowc} calculated as nm/(mg mL^{-1}), the trend is reversed (S_{lowc} nanoplastic > S_{lowc} microplastic), as reported in Table 2.

The binding kinetics were evaluated by monitoring the spectral shift at different time intervals for 8 min as shown in Figure 4 for all kinds of tested plastic particles. The response results were in accordance with the S_{lowc} values.

2.3. Plastic Particles Characterization via Artificial Intelligence. To meet the environmental challenge in the recognition and characterization of plastic particles,[29] an AI-based approach was applied to demonstrate the potential discriminations of size and composition. In fact, at varying size and type of plastic particles, the ER−SPR−POF response results are different, as reported in Section 2.2, hence paving the way to an ML-based approach for the classification. To this purpose, the prediction model was built using a standard Matlab toolbox called "Statistics and Machine Learning", which is a toolbox that offers a classification learner capable of training models and classify data. A known collection of data input and responses to those data were used in a supervised ML approach. Once the data was used to train the model, it made predictions about responses to the new data.

In this work, as a proof of concept, an ML-based model was developed to discriminate different plastic targets: nanoplastics (100 nm), and microplastics (20 μm), each tested in two different materials (PMMA and PS). Additionally, silica microparticles were selected as an example of nonplastic materials. These materials were chosen for their differences in the intrinsic physicochemical characteristics of materials and for their differences in terms of size.

The concentration of particles (plastic and nonplastic particles) was fixed at 3 mg/mL and the particles were tested one at a time in order to realize a proof-of-concept sensor system exploiting a reduction in the time of the training phase.

https://doi.org/10.1021/acsomega.3c09485
ACS Omega 2024, 9, 18984−18994

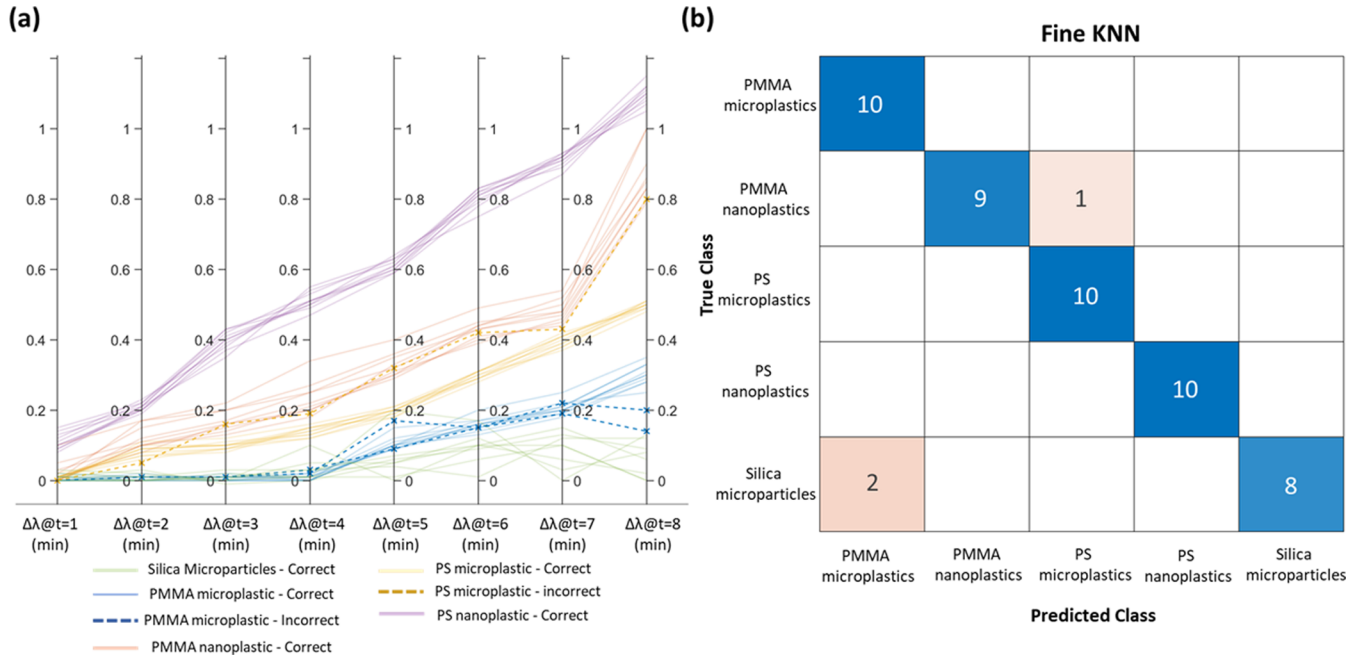

Figure 5. Plastic particles characterization based on AI: (a) Parallel coordinates plot relative to data set clustering and (b) confusion matrix obtained for the predictions over a stratified cross-validation procedure.

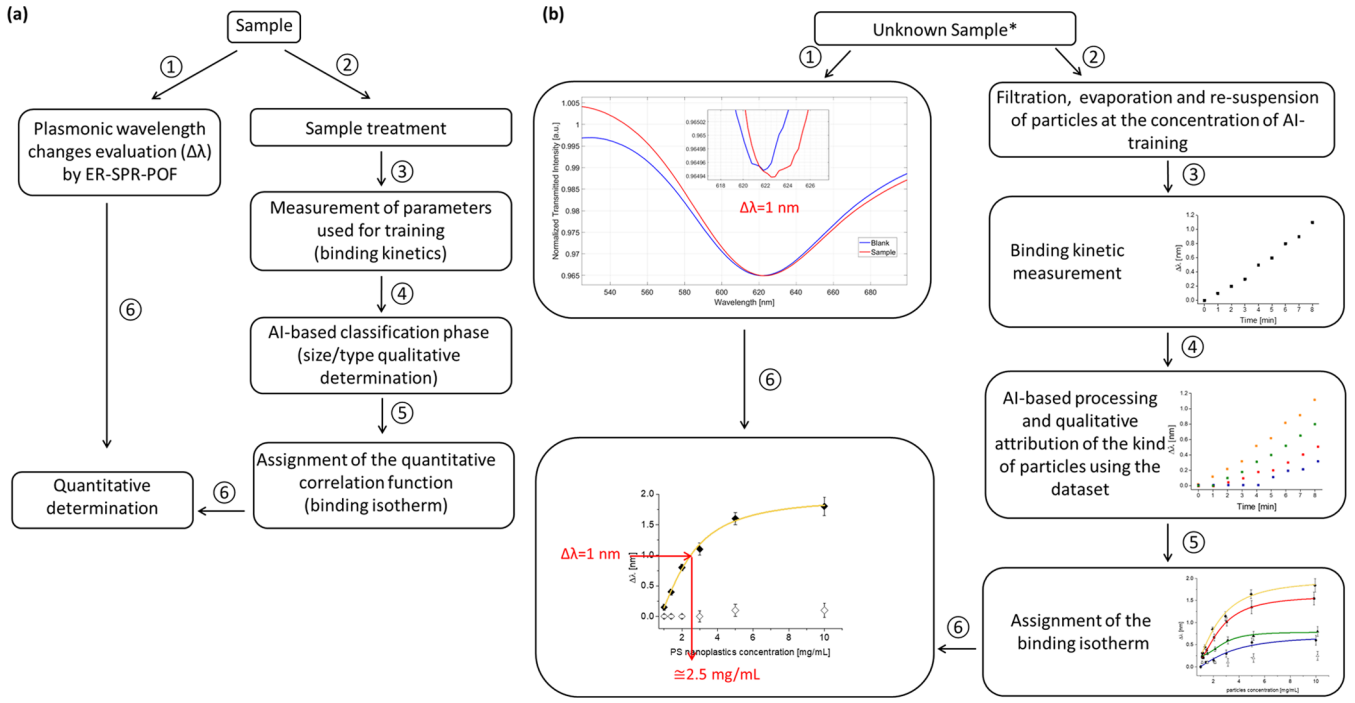

Figure 6. (a) Flowchart of the sensing scheme to characterize the plastic particles in terms of the concentration, size, and type. (b) Validation test of the AI−ER−SPR−POF method carried out with a spiked sample (*PS nanoplastics at 2.5 mg/mL).

The binding kinetics between plastic particles and ER, intended as variations of plasmonic wavelength ($\Delta\lambda$) registered at different incubation times each minute for 8 min as reported in Figure 4 (whole SPR spectra reported in Figure S4), were used as distinctive elements to build mathematical functions to train the algorithm. The measures were repeated (n = 10) for each sample, in order to build a data set adequately robust. Figure 5a plots the parallel coordinate plot showing the data set clustering results. In the silica microparticles case, the bioreceptor layer (ER) does not interact with this kind of particles.

In the next step, training of the classification algorithms, available from the Matlab toolbox, was performed. Among all, the K-nearest-neighbor (KNN) algorithm was chosen because it showed the highest accuracy (94%), as illustrated in the confusion matrix reported in Figure 5b.

Finally, the model obtained from the trained algorithm was applied to test blind solution types, providing as input data the resonance wavelength shifts (acquired every minute for 8 min).

https://doi.org/10.1021/acsomega.3c09485
ACS Omega 2024, 9, 18984−18994

The blind solutions were prepared by diluting different plastic particle stock solutions (PMMA and PS nanoplastics, PMMA and PS microplastics, and silica microparticles) at 3 mg/mL and were tested one at a time. The prediction results demonstrated an accuracy of 90.3%, paving the way for this type of approach for the classification of nano- and microplastics in terms of the size and material. The AI-based sensor systems depend on the data acquired during the training phase (data set). In this work, the mixtures of plastic particles were not used in the data set, so the proposed sensor system cannot identify these kinds of samples. In order to demonstrate this aspect, Figure S5 reports the results obtained by the binding kinetics relative to several mixtures. In particular, concerning the response for nonhomogeneous samples, the proposed sensor was tested for the following 50:50 mixtures of plastic particles at a fixed final concentration of 3 mg/mL (binding kinetics reported in Figure S5): PS nanoplastics/PMMA nanoplastics; PS nanoplastics/PS microplastics; and PS microplastics/PMMA nanoplastics. Hence, naturally, all of the tested mixtures of plastic particles are not correctly classified by the sensor system. In particular, the three nonhomogeneous solutions were incorrectly classified as PS nanoplastics, PS nanoplastics, and PMMA nanoplastics. In fact, as expected for these types of samples, the identification and classification system fails due to the simplified training fed to the AI. Instead, to identify even complex mixtures, it is necessary to expand the data set for AI training considerably or improve the algorithm's efficiency.[45−50]

2.4. Sensing Strategy to Evaluate the Size, Type, and Concentration of Plastic Particles: Validation of Unknown Samples. The sensing scheme outlined by the flowchart in Figure 6a shows that by exploiting the ML-based prediction model (Section 2.3) and the binding isotherm (Figure 3), it is possible to characterize unknown samples in terms of plastic particles concentration, size, and material. More specifically, a small sample fraction can be used to determine the SPR wavelength shift, whereas the remaining sample can be used to concentrate the plastic particles at the value used in the model training (3 mg/mL). This process can be performed by filtration and evaporation treatment and subsequent resuspension. Once the concentration is coherent with the kinetic data set, the trained model can predict the plastic particle size and material. Thus, the obtained result is then used to select the correct binding isotherm to extrapolate the concentration value from $\Delta\lambda$ achieved in the first phase ($\Delta\lambda$ measured for the untreated sample).

The qualitative and quantitative validation of this sensing strategy was carried out by testing a water sample added with PS nanoplastics with a theoretical concentration of 2.5 mg/mL (called the unknown sample, in Figure 6b).

In the first phase, a few microliters of the unknown sample (40 μL) were used to monitor the variation in resonance wavelength ($\Delta\lambda$) produced by the sample on the ER−SPR−POF sensor. Such $\Delta\lambda$ information is next used for quantitative determination.

In the second step, 5 mL of the unknown sample was treated by filtration and evaporation, followed by resuspension at the concentration used for training (3 mg/mL). 40 μL of the so-produced sample was placed on the ER−SPR−POF and the signal was registered each minute for 8 min. By the binding kinetics and from the KNN algorithm, the plastic particles in the unknown sample were then classified in terms of the size (micro/nano) and material (PMMA/PS). As a result, the sample was identified as PS nanoplastics.

Next, the quantification of the plastic particles in the unknown sample was attained by referring to the corresponding binding isotherm (Figure 3). By selecting the correct binding isotherm (PS nanoplastics) and using the $\Delta\lambda$ measured in the first step, a concentration of 2.5 mg/mL PS nanoplastics was obtained. The validation process is schematically summarized in Figure 6b.

Moreover, in order to support the possibility of using the sensing strategy in different matrices, the validation was also performed in simulated seawater for a spiked sample, as reported in Section S6.

It should be stressed that, by utilizing highly sensitive plasmonic platforms, like the one based on gold nanograting (GNG) recently presented in Seggio et al.[40] for plastic particles detection at an ultralow concentration range, the same AI-based strategy here discussed could be used to detect plastic particles in a different concentration range (e.g., ng/mL). Nevertheless, in this work, considering the expensive and time-consuming GNG production process and the need for a discrete amount of sensing platforms to adequately build the data set, a cheaper technology (the SPR−POF probes) was chosen to demonstrate the capabilities of the proposed approach.

3. DISCUSSION AND CONCLUSIONS

Optical and electrochemical sensing strategies integrated with discrimination capability for the particle size and type represent a growing field.[51,52] In particular, different optical and/or electrochemical platforms were developed for this purpose.[53−61] For instance, the coupling between optical tweezers and ML was demonstrated for microplastics classification in terms of both size and material.[53] However, this approach was not proven for plastic nanoparticles and requires an expensive and complex experimental setup. Along this line, Doi et al.[54] demonstrated the use of optical tweezers to distinguish nano- and microparticles but without the discrimination of the material type. A very recent work[55] proposes a sensing approach by hyperspectral stimulated Raman scattering (SRS) microscopy, demonstrating the nanoplastics classification in terms of different materials in water samples,[55] but in this case too, the approach requires complex and expensive instrumentation. Analytical methods for microplastics characterization exploiting FTIR analysis coupled with AI-based tools were also available.[56,57] Additionally, the use of surface enhanced Raman scattering (SERS) substrates paves the way for micro- and nanoplastics identification.[58] Lv et al.[59] utilized a SERS substrate able to effectively detect plastic particles of different sizes and materials in water samples, despite the fact that any kind of AI-based classification was performed.

So far, none of these approaches have been reported for simultaneous identification and classification of both nano- and microplastics in terms of size and material on one single sensor.

In this work, we reported the development of a plasmonic biosensor coupled with the ER receptor, the latter suitable to bind micrometric and submicrometric plastic fragments. This recognition element was chosen because the literature reported it as suitable for the detection of different microplastics via a conventional SPR device.[38] The interaction between the ER and the microplastics is mainly hydrophobically driven.[38] It was reported that different kinds of microplastics interacted

https://doi.org/10.1021/acsomega.3c09485
ACS Omega 2024, 9, 18984−18994

with the ER in a slightly different manner, according to their physicochemical characteristics, and hence were characterized by specific kinetics.[38] Thus, the ER plasmonic surface was apt for the recent definition of "MathMaterial interface",[62] which is a nonspecific interface exploited for its ability to sense different types of analytes by means of a quasi-nonspecific sensing layer.

The sets of changes occurring to the ER in response to different analytes resulted in specific and distinctive functions that ultimately produced specific patterns of signals, as suggested by the variation of plasmonic resonance wavelength at different times shown in Figure 5a. Here, the interactions of the ER receptor to the plastic fragment that resulted in the distinguished mathematical functions in dependence on the changes in the plastic size (micro/nano) and type of plastic material (PMMA and PS) were fed to an AI algorithm for size- and type-dependent categorization. Additionally, it is envisaged that the ER-based sensor would broaden or restrict the selectivity by optimizing training algorithms and/or the data set.

It should be stressed that in the specific detection of substances based on nonspecific receptors combined with AI, the ML-based prediction model efficiency in terms of sensor selectivity can be improved by optimizing the training algorithms[45−47] and/or the data set.[48−50]

In this work, it has been shown that the ER−SPR−POF responds with different functions to each type of tested plastic particle.[38]

In the present work, a novel strategy to detect, classify, and quantify the plastic particles in terms of the size and material was proposed. In fact, in addition to the capability to detect plastic particles with different sizes (micro- and nano-) and materials (PMMA and PS), we also provide an ML-based strategy (schematized in Figure 6) to classify and then quantify the plastic particles content in water samples.

Along this line, the future perspective foresees to test several plastic particles, both one at a time and in mixtures at different ratios and in different matrices, in order to expand the data set to train the algorithm to obtain a sensor capable of detecting and identifying nonhomogeneous plastic particle samples present in a real scenario.

4. MATERIALS AND METHODS

4.1. List of Chemicals. Recombinant human estrogen receptor α protein (ER) (ab82606 abcam) was purchased from Abcam (Cambridge, U.K.). Poly(methyl methacrylate) (PMMA) nanoplastics (100 nm) (DNP-P034) and microplastic (20 μm) (DMN-L015) and polystyrene (PS) nanoplastics (100 nm) (DNT-B010) and microplastics (20 μm) (DNT-B20) were purchased from CD Bioparticles (London, U.K.) as a standard aqueous stock solution (10 mg/mL). Silica microparticles 40−63 μm particle size (112926-00-8), *N*-hydroxysuccinimide (NHS) (6066-82-6), *N*-(3-(dimethylamino)propyl)-*N*′-ethylcarbodiimide hydrochloride (EDC) (25952-53-8), α-lipoic acid (1077-28-7), ethanolamine (141-43-5), phosphate buffered saline 10 mM, pH 7.4 (PBS) (MFCD00131855), and 2-(*N*-morpholino)ethanesulfonic acid (MES) (4432-31-9) were purchased from Sigma-Aldrich (Darmstadt, Germany).

4.2. POF-Based Plasmonic Chip. The SPR−POF platform fabrication is extensively described by Cennamo et al.[41] Briefly, a POF is embedded in a resin support and polished with papers (5 and 1 μm grits) to realize the D-shaped POF area (l = 10 mm). Subsequently, a photoresist buffer layer (Microposit S1813, MicroChem Corp., Westborough, MA) is spin-coated to improve the optical performance.[41] Finally, a 60 nm gold film is deposited by a sputter coater machine (Safematic CCU-010, Zizers, Switzerland). The fabrication scheme is summarized in Figure 1a. The planar sensing surface of the chip (10 mm × 1 mm) can be used to carry out the measurements by dropping the sample solution without microfluidic cells.

4.3. ER Functionalization Protocol. The functionalization of the plasmonic platform was performed according to the protocol reported by Arcadio et al.[42] and optimized by Pasquardini et al.[43] The gold surface, previously washed with Milli-Q water, was treated overnight at room temperature with α-lipoic acid (0.3 mM in 8% ethanolic solution) to let the thiol groups react with the gold surfaces. The so-produced self-assembled monolayer (SAM) with a carboxylic terminal group was activated with EDC/NHS (both 10 mM) in MES buffer 50 mM pH 5.5, for 20 min at room temperature.

After washing to remove the reactant in excess, the surface was incubated for 2 h with ER (30 ng) at room temperature in a sealed humid box for covalent immobilization of the receptor. Finally, the passivation of the surface was performed by incubating ethanolamine (1 mM) for 30 min at room temperature, in order to passivate unreacted activated carboxylic groups. The prepared platforms were washed and stored in PBS at 4 °C. The scheme of the platforms' functionalization is reported in Figure 1b.

4.4. Analysis of ER−SPR−POF by ATR-FTIR. Attenuated total reflectance (ATR)-FTIR spectra were recorded with a Thermo Fisher Scientific Nicolet iS50 FTIR Spectrometer in the mid-IR range, subtracting the contribution from air (blank), and collecting 32 scans for each spectrum with a resolution of 4 cm^{-1}.

4.5. Measurement Setup. To test the SPR platform, a simple experimental setup consisting of a halogen lamp with an emission range 360−1700 nm (HL-2000LL, Ocean Insight, Orlando, FL) and a spectrometer with a detection range 350−1000 nm (FLAME-S-VIS-NIR-ES, Ocean Insight, Orlando, FL) was used. The SPR−POF platform was connected to the light source and spectrometer through SMA connectors. The POF used to build the plasmonic platform is not bending-insensitive. Hence, to avoid a possible effect induced by mechanical deformations, the SPR−POF platform was embedded in a resin cube (as shown in the scheme in Figure 1a) that was immobilized in a 3D-printed holder as shown in Figure 1c. Finally, the spectrometer is connected to a PC by a USB cable.

4.6. Measurement Procedures of Binding Isotherms. Micro- and nanoplastic stock solutions were diluted to the final tested concentrations (ranging from 1 to 10 mg/mL) with water. Prior to use, all solutions were always sonicated for ∼15 min to ensure micro- and nanoplastics were homogeneously dispersed. Measurements were performed by placing 40 μL of the sample on the sensor and incubating the sample for 8 min. The plasmonic spectra were collected after a washing step by placing water (40 μL) as a bulk solution. The spectrum acquired with air as a surrounding medium was considered as a reference spectrum for the normalization since the plasmonic phenomenon is not triggered.[41] Error bars were calculated as the maximum experimentally measured variation obtained by testing three similar platforms under similar conditions.

4.7. Analysis via Artificial Intelligence. The ER−SPR−POF platform was tested by monitoring the wavelength shifts

https://doi.org/10.1021/acsomega.3c09485
ACS Omega 2024, 9, 18984−18994

over time for 8 min and for the different solutions, i.e., PMMA and PS nanoplastic (100 nm), PMMA and PS microplastics (20 μm), and silica microparticles (40−63 μm), all considered at a fixed concentration equal to 3 mg/mL. All measurements were performed under fixed conditions of temperature (25 °C) and in Milli-Q water. In fact, changes in the environmental conditions in terms of temperature or matrix produce differences in the interaction of plastic particles with ER (the recognition layer),[63] and the phenomenon would lead the algorithm to miss in recognizing. To mitigate this aspect, the training phase of the sensor system could be expanded with a greater number of samples by considering these environmental conditions (in terms of temperature or matrix) in order to use the sensor in a real scenario.

The resonance wavelength shifts ($\Delta\lambda$) were acquired at each minute, for 8 min of incubation time, for each tested solution. The acquisition was repeated 10 times for each sample to build a robust data set to accurately train and validate the prediction model. The prediction model was carried out using a standard Matlab toolbox named as "Statistics and Machine Learning" and choosing the K-nearest-neighbor (KNN) algorithm.

■ ASSOCIATED CONTENT

Supporting Information

The Supporting Information is available free of charge at https://pubs.acs.org/doi/10.1021/acsomega.3c09485.

> Whole SPR spectra used to carry out the binding isotherm; SPR spectra obtained on bare platforms; binding isotherm reported in molar concentration; whole spectra of binding kinetics and binding kinetics of nonhomogeneous samples; validation of plastic particle classification in simulated seawater samples (PDF)

■ AUTHOR INFORMATION

Corresponding Author

Mimimorena Seggio − *Department of Biotechnology, University of Verona, 37134 Verona, Italy;* orcid.org/0000-0002-8193-5873; Email: mimimorena.seggio@univr.it

Authors

Francesco Arcadio − *Department of Engineering, University of Campania Luigi Vanvitelli, 81031 Aversa, Italy;* orcid.org/0000-0001-7863-743X

Eros Radicchi − *Department of Biotechnology, University of Verona, 37134 Verona, Italy;* orcid.org/0000-0003-0749-3824

Nunzio Cennamo − *Department of Engineering, University of Campania Luigi Vanvitelli, 81031 Aversa, Italy*

Luigi Zeni − *Department of Engineering, University of Campania Luigi Vanvitelli, 81031 Aversa, Italy*

Alessandra Maria Bossi − *Department of Biotechnology, University of Verona, 37134 Verona, Italy;* orcid.org/0000-0002-2542-8412

Complete contact information is available at: https://pubs.acs.org/10.1021/acsomega.3c09485

Author Contributions

[§]M.S. and F.A. contributed equally to this work. The manuscript was written through contributions of all authors. All authors have given approval to the final version of the manuscript. M.S.: conceptualization, investigation, methodology, data curation, writing—original draft, writing—review and editing; F.A.: conceptualization, investigation, methodology, data curation, writing—original draft, writing—review and editing; E.R.: investigation, methodology, data curation; C.N.: conceptualization, methodology, supervision, writing—original draft, writing—review and editing; L.Z.: supervision, funding acquisition, writing—review and editing; A.M.B.: conceptualization, methodology, funding acquisition, supervision, writing—original draft, writing—review and editing.

Notes

The authors declare no competing financial interest.

■ ACKNOWLEDGMENTS

N.C., F.A., and L.Z. thank the MUR—PRIN 2022 "BOHEMIAN"—(CUP: B53D23002680006) Italian Project; M.S. and A.M.B. thank the Italian Ministry of University for the Project DM 1062 2021 "Ricercatori a Tempo Determinato di tipo A (RTDA) Azione IV.6—Contratti di ricerca su tematiche Green" awarded to M.S. [40-G-15185-5]. E.R. thanks the Italian Ministry of University for the Project DM 1062 2021 "Ricercatori a Tempo Determinato di tipo A (RTDA) Azione IV.6—Contratti di ricerca su tematiche Green" [40-G-15185-4]. This work has been conducted in part within the research program "Dipartimento di Eccellenza 2023−2027" awarded to Dipartimento di Biotecnologie of the Università di Verona.

■ REFERENCES

(1) Tittl, A.; John-Herpin, A.; Leitis, A.; Arvelo, E. R.; Altug, H. Metasurface-Based Molecular Biosensing Aided by Artificial Intelligence. *Angew. Chem., Int. Ed.* **2019**, *58*, 14810−14822.

(2) Jin, X.; Liu, C.; Xu, T.; Su, L.; Zhang, X. Artificial Intelligence Biosensors: Challenges and Prospects. *Biosens. Bioelectron.* **2020**, *165*, No. 112412.

(3) Arya, S. S.; Dias, S. B.; Jelinek, H. F.; Hadjileontiadis, L. J.; Pappa, A.-M. The Convergence of Traditional and Digital Biomarkers through AI-Assisted Biosensing: A New Era in Translational Diagnostics? *Biosens. Bioelectron.* **2023**, *235*, No. 115387.

(4) Pouyanfar, N.; Harofte, S. Z.; Soltani, M.; Siavashy, S.; Asadian, E.; Ghorbani-Bidkorbeh, F.; Keçili, R.; Hussain, C. M. Artificial Intelligence-Based Microfluidic Platforms for the Sensitive Detection of Environmental Pollutants: Recent Advances and Prospects. *Trends Environ. Anal. Chem.* **2022**, *34*, No. e00160.

(5) Cho, S.-Y.; Lee, Y.; Lee, S.; Kang, H.; Kim, J.; Choi, J.; Ryu, J.; Joo, H.; Jung, H.-T.; Kim, J. Finding Hidden Signals in Chemical Sensors Using Deep Learning. *Anal. Chem.* **2020**, *92*, 6529−6537.

(6) Ballard, Z.; Brown, C.; Madni, A. M.; Ozcan, A. Machine Learning and Computation-Enabled Intelligent Sensor Design. *Nat. Mach. Intell.* **2021**, *3*, 556−565.

(7) Di Natale, C.; Paolesse, R.; Macagnano, A.; Mantini, A.; D'Amico, A.; Legin, A.; Lvova, L.; Rudnitskaya, A.; Vlasov, Y. Electronic Nose and Electronic Tongue Integration for Improved Classification of Clinical and Food Samples. *Sens. Actuators, B* **2000**, *64*, 15−21.

(8) Chen, X.; Xu, Y.; Meng, L.; Chen, X.; Yuan, L.; Cai, Q.; Shi, W.; Huang, G. Non-parametric partial least squares—Discriminant analysis model based on sum of ranking difference algorithm for tea grade identification using electronic tongue data. *Sens. Actuators, B* **2020**, *311*, No. 127924.

(9) Schackart, K. E.; Yoon, J.-Y. Machine Learning Enhances the Performance of Bioreceptor-Free Biosensors. *Sensors* **2021**, *21*, No. 5519.

(10) Hotel, O.; Poli, J.-P.; Mer-Calfati, C.; Scorsone, E.; Saada, S. A review of algorithms for SAW sensors Enose based volatile compound identification. *Sens. Actuators, B* **2018**, *255*, 2472−2482.

(11) Leon-Medina, J. X.; Anaya, M.; Pozo, F.; Tibaduiza, D. Nonlinear Feature Extraction Through Manifold Learning in an Electronic Tongue Classification Task. *Sensors* **2020**, *20*, No. 4834.
(12) Daliri, M. R. Combining extreme learning machines using support vector machines for breast tissue classification. *Comput. Methods Biomech. Biomed. Eng.* **2015**, *18*, 185−191.
(13) Huang, G.-B.; Zhu, Q.-Y.; Siew, C.-K. Extreme learning machine: Theory and applications. *Neurocomputing* **2006**, *70*, 489−501.
(14) Szulczyński, B.; Armiński, K.; Namiesnik, J.; Gębicki, J. Determination of odour interactions in gaseous mixtures using electronic nose methods with artificial neural networks. *Sensors* **2018**, *18*, No. 519.
(15) Materić, D.; Kasper-Giebl, A.; Kau, D.; Anten, M.; Greilinger, M.; Ludewig, E.; van Sebille, E.; Röckmann, T.; Holzinger, R. Micro- and Nanoplastics in Alpine Snow: A New Method for Chemical Identification and (Semi)Quantification in the Nanogram Range. *Environ. Sci. Technol.* **2020**, *54*, 2353−2359.
(16) Kanhai, L. D. K.; Gardfeldt, K.; Krumpen, T.; Thompson, R. C.; O'Connor, I. Microplastics in Sea Ice and Seawater beneath Ice Floes from the Arctic Ocean. *Sci. Rep.* **2020**, *10*, No. 5004.
(17) Kelly, A.; Lannuzel, D.; Rodemann, T.; Meiners, K. M.; Auman, H. J. Microplastic Contamination in East Antarctic Sea Ice. *Mar. Pollut. Bull.* **2020**, *154*, No. 111130.
(18) Allen, D.; Allen, S.; Le Roux, G.; Simonneau, A.; Galop, D.; Phoenix, V. R. Temporal Archive of Atmospheric Microplastic Deposition Presented in Ombrotrophic Peat. Environ. *Sci. Technol. Lett.* **2021**, *8*, 954−960.
(19) Wahl, A.; Le Juge, C.; Davranche, M.; El Hadri, H.; Grassl, B.; Reynaud, S.; Gigault, J. Nanoplastic Occurrence in a Soil Amended with Plastic Debris. *Chemosphere* **2021**, *262*, No. 127784.
(20) Bergmann, M.; Wirzberger, V.; Krumpen, T.; Lorenz, C.; Primpke, S.; Tekman, M. B.; Gerdts, G. High Quantities of Microplastic in Arctic Deep-Sea Sediments from the Hausgarten Observatory. *Environ. Sci. Technol.* **2017**, *51*, 11000−11010.
(21) de las Hazas, M.-C. L.; Boughanem, H.; Dávalos, A. Untoward Effects of Micro- and Nanoplastics: An Expert Review of Their Biological Impact and Epigenetic Effects. *Adv. Nutr.* **2022**, *13*, 1310−1323.
(22) Geyer, R.; Jambeck, J. R.; Law, K. L. Production, Use, and Fate of All Plastics Ever Made. *Sci. Adv.* **2017**, *3*, No. e1700782.
(23) PlasticsEurope. *An Analysis of European Plastics Production, Demand and Waste Data* PlasticsEurope: Brussels, Belgium; 2019.
(24) Science for Environment Policy. Nanoplastics: state of knowledge and environmental and human health impacts. Issue 27. Produced for European Commission DG Environment by the Science Communication Unit, UWE Bristol, 2023. https://ec.europa.eu/scienceenvironment-policy.
(25) Wright, S. L.; Kelly, F. J. Plastic and Human Health: A Micro Issue? *Environ. Sci. Technol.* **2017**, *51*, 6634−6647.
(26) Bianco, A.; Sordello, F.; Ehn, M.; Vione, D.; Passananti, M. Degradation of Nanoplastics in the Environment: Reactivity and Impact on Atmospheric and Surface Waters. *Sci. Total Environ.* **2020**, *742*, No. 140413.
(27) Bond, T.; Ferrandiz-Mas, V.; Felipe-Sotelo, M.; van Sebille, E. The Occurrence and Degradation of Aquatic Plastic Litter Based on Polymer Physicochemical Properties: *A Review*. *Crit. Rev. Environ. Sci. Technol.* **2018**, *48*, 685−722.
(28) Hartmann, N. B.; Hüffer, T.; Thompson, R. C.; Hassellöv, M.; Verschoor, A.; Daugaard, A. E.; Rist, S.; Karlsson, T.; Brennholt, N.; Cole, M.; et al. Are We Speaking the Same Language? Recommendations for a Definition and Categorization Framework for Plastic Debris. *Environ. Sci. Technol.* **2019**, *53*, 1039−1047.
(29) Silva, A. B.; Bastos, A. S.; Justino, C. I. L.; da Costa, J. P.; Duarte, A. C.; Rocha-Santos, T. A. P. Microplastics in the Environment: Challenges in Analytical Chemistry - A Review. *Anal. Chim. Acta* **2018**, *1017*, 1−19.
(30) Delgado-Gallardo, J.; Sullivan, G. L.; Esteban, P.; Wang, Z.; Arar, O.; Li, Z.; Watson, T. M.; Sarp, S. From Sampling to Analysis: A Critical Review of Techniques Used in the Detection of Micro- and Nanoplastics in Aquatic Environments. *ACS EST Water* **2021**, *1*, 748−764.
(31) Ivleva, N. P. Chemical Analysis of Microplastics and Nanoplastics: Challenges, Advanced Methods, and Perspectives. *Chem. Rev.* **2021**, *121*, 11886−11936.
(32) Martic, S.; Tabobondung, M.; Gao, S.; Lewis, T. Emerging Electrochemical Tools for Microplastics Remediation and Sensing. *Front. Sens.* **2022**, *3*, No. 958633.
(33) Xu, H.; Zheng, W.; Zhang, Y.; Zhao, D.; Wang, L.; Zhao, Y.; Wang, W.; Yuan, Y.; Zhang, J.; Huo, Z.; Wang, Y.; Zhao, N.; Qin, Y.; Liu, K.; Xi, R.; Chen, G.; Zhang, H.; Tang, C.; Yan, J.; Ge, Q.; Cheng, H.; Lu, Y.; Gao, L. A Fully Integrated, Standalone Stretchable Device Platform with in-Sensor Adaptive Machine Learning for Rehabilitation. *Nat. Commun.* **2023**, *14*, No. 7769.
(34) Zhu, Z.; Guo, S.-Z.; Hirdler, T.; Eide, C.; Fan, X.; Tolar, J.; McAlpine, M. C. 3D Printed Functional and Biological Materials on Moving Freeform Surfaces. *Adv. Mater.* **2018**, *30*, No. 1707495.
(35) Zheng, B.; Zhao, G.; Yan, Z.; Xie, Y.; Lin, J. Direct Freeform Laser Fabrication of 3D Conformable Electronics. *Adv. Funct. Mater.* **2023**, *33*, No. 2210084.
(36) Yi, N.; Gao, Y.; Lo Verso, A., Jr; Zhu, J.; Erdely, D.; Xue, C.; Lavelle, R.; Cheng, H. Fabricating Functional Circuits on 3D Freeform Surfaces via Intense Pulsed Light-Induced Zinc Mass Transfer. *Mater. Today* **2021**, *50*, 24−34.
(37) Hong, S. H.; Chen, T.; Wang, G.; Popovic, S. M.; Filleter, T.; Naguib, H. E. Room-Temperature Self-Healing Polysiloxane Networks for Highly Sensitive Piezoresistive Pressure Sensor with Microdome Structures. *J. Chem. Eng.* **2023**, *471*, No. 144429.
(38) Huang, C.-J.; Narasimha, G. V.; Chen, Y.-C.; Chen, J.-K.; Dong, G.-C. Measurement of Low Concentration of Micro-Plastics by Detection of Bioaffinity-Induced Particle Retention Using Surface Plasmon Resonance Biosensors. *Biosensors* **2021**, *11*, No. 219.
(39) Tuoriniemi, J.; Moreira, B.; Safina, G. Determining Number Concentrations and Diameters of Polystyrene Particles by Measuring the Effective Refractive Index of Colloids Using Surface Plasmon Resonance. *Langmuir* **2016**, *32*, 10632−10640.
(40) Seggio, M.; Arcadio, F.; Cennamo, N.; Zeni, L.; Bossi, A. M. A Plasmonic Gold Nano-Surface Functionalized with the Estrogen Receptor for Fast and Highly Sensitive Detection of Nanoplastics. *Talanta* **2024**, *267*, No. 125211.
(41) Cennamo, N.; Massarotti, D.; Conte, L.; Zeni, L. Low Cost Sensors Based on SPR in a Plastic Optical Fiber for Biosensor Implementation. *Sensors* **2011**, *11*, 11752−11760.
(42) Arcadio, F.; Seggio, M.; Zeni, L.; Bossi, A. M.; Cennamo, N. Estradiol Detection for Aquaculture Exploiting Plasmonic Spoon-Shaped Biosensors. *Biosensors* **2023**, *13*, No. 432.
(43) Pasquardini, L.; Cennamo, N.; Malleo, G.; Vanzetti, L.; Zeni, L.; Bonamini, D.; Salvia, R.; Bassi, C.; Bossi, A. M. A Surface Plasmon Resonance Plastic Optical Fiber Biosensor for the Detection of Pancreatic Amylase in Surgically-Placed Drain Effluent. *Sensors* **2021**, *21*, No. 3443.
(44) Enyoh, C. E.; Wang, Q.; Ovuoraye, P. E.; Maduka, T. O. Toxicity Evaluation of Microplastics to Aquatic Organisms through Molecular Simulations and Fractional Factorial Designs. *Chemosphere* **2022**, *308*, No. 136342.
(45) Ozcift, A.; Gulten, A. Classifier Ensemble Construction with Rotation Forest to Improve Medical Diagnosis Performance of Machine Learning Algorithms. *Comput. Methods Prog. Biomed.* **2011**, *104*, 443−451.
(46) Bui, D. T.; Khosravi, K.; Tiefenbacher, J.; Nguyen, H.; Kazakis, N. Improving Prediction of Water Quality Indices Using Novel Hybrid Machine-Learning Algorithms. *Sci. Total Environ.* **2020**, *721*, No. 137612.
(47) Wang, Y.; Xing, J.; Qian, S. Selectivity Enhancement in Electronic Nose Based on an Optimized DQN. *Sensors* **2017**, *17*, No. 2356.
(48) Xiao, X.; Min, J.-L.; Lin, W.-Z.; Liu, Z.; Cheng, X.; Chou, K.-C. iDrug-Target: Predicting the Interactions between Drug Compounds

https://doi.org/10.1021/acsomega.3c09485
ACS Omega 2024, 9, 18984−18994

and Target Proteins in Cellular Networking via Benchmark Dataset Optimization Approach. *J. Biomol. Struct. Dyn.* **2015**, *33*, 2221−2233.
(49) Massaro, A.; Maritati, V.; Giannone, D.; Convertini, D.; Galiano, A. LSTM DSS Automatism and Dataset Optimization for Diabetes Prediction. *Appl. Sci.* **2019**, *9*, No. 3532.
(50) Jia, J.; Liu, Z.; Xiao, X.; Liu, B.; Chou, K.-C. iPPBS-Opt: A Sequence-Based Ensemble Classifier for Identifying Protein-Protein Binding Sites by Optimizing Imbalanced Training Datasets. *Molecules* **2016**, *21*, No. 95.
(51) Fang, C.; Luo, Y.; Naidu, R. Microplastics and Nanoplastics Analysis: Options, Imaging, Advancements and Challenges. *TrAC Trends Anal. Chem.* **2023**, *166*, No. 117158.
(52) Fang, C.; Luo, Y.; Naidu, R. Advancements in Raman Imaging for Nanoplastic Analysis: Challenges, Algorithms and Future Perspectives. *Anal. Chim. Acta* **2024**, *1290*, No. 342069.
(53) Carvalho, I. A.; Silva, N. A.; Rosa, C. C.; Coelho, L. C. C.; Jorge, P. A. S. Particle Classification through the Analysis of the Forward Scattered Signal in Optical Tweezers. *Sensors* **2021**, *21*, No. 6181.
(54) Doi, K.; Yamamoto, K.; Yamazaki, H.; Kawano, S. Micro-to-Nano Bimodal Single-Particle Sensing Using Optical Tweezers. *J. Phys. Chem. C* **2022**, *126*, 10713−10721.
(55) Qian, N.; Gao, X.; Lang, X.; Deng, H.; Bratu, T. M.; Chen, Q.; Stapleton, P.; Yan, B.; Min, W. Rapid Single-Particle Chemical Imaging of Nanoplastics by SRS Microscopy. *Proc. Natl. Acad. Sci. U.S.A.* **2024**, *121*, No. e2300582121.
(56) da Silva, V. H.; Murphy, F.; Amigo, J. M.; Stedmon, C.; Strand, J. Classification and Quantification of Microplastics (<100 μm) Using a Focal Plane Array−Fourier Transform Infrared Imaging System and Machine Learning. *Anal. Chem.* **2020**, *92*, 13724−13733.
(57) Brandt, J.; Mattsson, K.; Hassellöv, M. Deep Learning for Reconstructing Low-Quality FTIR and Raman Spectra—A Case Study in Microplastic Analyses. *Anal. Chem.* **2021**, *93*, 16360−16368.
(58) Chen, Q.; Wang, J.; Yao, F.; Zhang, W.; Qi, X.; Gao, X.; Liu, Y.; Wang, J.; Zou, M.; Liang, P. A Review of Recent Progress in the Application of Raman Spectroscopy and SERS Detection of Microplastics and Derivatives. *Microchim. Acta* **2023**, *190*, No. 465.
(59) Lv, L.; He, L.; Jiang, S.; Chen, J.; Zhou, C.; Qu, J.; Lu, Y.; Hong, P.; Sun, S.; Li, C. In Situ Surface-Enhanced Raman Spectroscopy for Detecting Microplastics and Nanoplastics in Aquatic Environments. *Sci. Total Environ.* **2020**, *728*, No. 138449.
(60) Han, Y.; Ding, L.; Wang, Y.; Zheng, H.; Fang, L. Shape Discrimination of Individual Aerosol Particles Using Light Scattering. *Sensors* **2023**, *23*, No. 5464.
(61) Vogel, R.; Willmott, G.; Kozak, D.; Roberts, G. S.; Anderson, W.; Groenewegen, L.; Glossop, B.; Barnett, A.; Turner, A.; Trau, M. Quantitative Sizing of Nano/Microparticles with a Tunable Elastomeric Pore Sensor. *Anal. Chem.* **2011**, *83*, 3499−3506.
(62) Cennamo, N.; Arcadio, F.; Capasso, F.; Maniglio, D.; Zeni, L.; Bossi, A. M. Non-Specific Responsive Nanogels and Plasmonics to Design MathMaterial Sensing Interfaces: The Case of a Solvent Sensor. *Sensors* **2022**, *22*, No. 10006.
(63) Notides, A. C. Binding Affinity and Specificity of the Estrogen Receptor of the Rat Uterus and Anterior Pituitary. *Endocrinology* **1970**, *87*, 987−992.

https://doi.org/10.1021/acsomega.3c09485
ACS Omega 2024, 9, 18984−18994